Optimization of the Pechini-derived synthesis of rare-earth free aluminum borate phosphors presenting tunable white emission

Jérémy Cathalan, Mathieu Salaün, Pierre Gaffuri, Audrey Potdevin, François Réveret, Alain Ibanez, Geneviève Chadeyron, Isabelle Gautier-Luneau

J Mater Sci

Electronic materials

Optimization of the Pechini-derived synthesis of rare-earth free aluminum borate phosphors presenting tunable white emission

Jérémy Cathalan[1,2], Mathieu Salaün[1,*], Pierre Gaffuri[1], Audrey Potdevin[2], François Réveret[2], Alain Ibanez[1], Geneviève Chadeyron[2], and Isabelle Gautier-Luneau[1,*]

[1] *Univ. Grenoble Alpes, CNRS, Grenoble INP, Institut Néel, 38000 Grenoble, France*
[2] *Université Clermont Auvergne, Clermont Auvergne INP, CNRS, Institut de Chimie de Clermont-Ferrand, 63000 Clermont-Ferrand, France*

Received: 4 June 2022
Accepted: 7 August 2022

ABSTRACT

The present study is dedicated to the development of aluminum borate luminescent powders which appear as promising and more environmental-friendly than conventional phosphors. The different steps of the luminescent powder synthesis, in particular the precursors (inorganic and organic) ratios and calcination conditions, are adjusted by studying the resulting optical features to get a broader and warmer white emission. As shown in previous works, the photoluminescence emission originates from polyaromatic hydrocarbons trapped in the inorganic aluminum borate matrix. Morphological and structural properties of the particles remain otherwise identical for every optimized parameter. The aluminum borate powder synthesized in these optimized conditions exhibits a wide and intense emission band under near-UV excitation. These structural and optical properties combined with time-resolved photoluminescence measurements demonstrate that the adjustments of the synthetic process allow the formation and trapping of more and different emitting centers. The modulation of the excitation wavelength (from 305 to 405 nm) leads to a tunable photoluminescence emission characterized by a large band lying between 400 and 700 nm. This feature, associated with the use of secure and abundant precursors makes aluminum borate powders very interesting phosphors for optical applications.

Handling Editor: Till Froemling.

Address correspondence to E-mail: mathieu.salaun@neel.cnrs.fr; Isabelle.Gautier-Luneau@neel.cnrs.fr

https://doi.org/10.1007/s10853-022-07619-5

Introduction

Solid-state white light displays using light emitting diodes (LEDs) have emerged over the last decade and they are substituting traditional technologies thanks to a significantly reduced energy consumption. The phosphor-converted (pc)-White LEDs (WLEDs) usually combine a semiconductor chip emitting in the ultraviolet or blue wavelength range to one or more phosphor(s) generally deposited in the form of coatings using either on-chip or remote configurations [1]. Herein, we will focus on the last one.

Commonly commercialized pc-WLEDs are composed of a blue-emitting InGaN LED covered by a composite material made of a polymeric matrix in which a mixture of luminescent compounds is dispersed: the yellow phosphor cerium-doped yttrium aluminum garnet ($Y_3Al_5O_{12}:Ce^{3+}$ or YAG:Ce) [2–4] usually blended with a red phosphor (generally Eu^{2+} doped nitride or sulfide compounds) to convert the chip emission into a warm white emission [5–7].

More recently, the use of near-UV LEDs as excitation sources has attracted a lot of attention in order to optimize photometric parameters such as color rendering index (CRI) or correlated color temperature (CCT). Several strategies are exposed in the literature: the most common consists in the association of the UV LED with red, green and blue (RGB) phosphors to generate an overall white light. Two approaches for the mixture of colors are then considered. The first one involves the mixture of the three RGB phosphors to prepare a one-layer coating with a broad emission band covering the entire visible spectrum [8, 9]. The second process is based on the superposition of three layers of single-color phosphors: phosphor powder dispersed in a polymeric matrix or phosphor in glass. Major issues of cascade-excitation resulting in a low luminous efficacy are raised [8, 10], an important optimization work has to be done to reduce this phenomenon. Another way to obtain white light using UV LED is to combine it with a suitably doped (Eu^{2+}, Eu^{3+}, Dy^{3+}) or co-doped ($Tm^{3+}/Tb^{3+}/Eu^{3+}$, Tm^{3+}/Dy^{3+}, $Yb^{3+}/Er^{3+}/Tm^{3+}$) single-phase host such as silicates, phosphates or even oxychlorides [11].

Both blue- and UV-excitation systems aforementioned lift two main drawbacks: an instability of their photometric parameters due to temperature aging and the use of rare-earths (RE) in phosphors composition (yttrium, cerium, europium…) [4, 12–14]. These latter have been classified as critical elements by the European Union [15]. The ore extraction requires important quantities of chemicals, water and energy [16, 17], and it is thus associated with environmental and economic issues [17–19]. Most of the generated pollution results from the storage of the residues from the ore refining. The wastewaters and processed chemicals are stored in huge open air retention basins. Among these toxic spills, we can cite heavy metals and radioactive elements: soil, air and surface/groundwater can be contaminated in large areas around the mines [20–22]. Hence, developing alternative phosphors to overcome these issues is getting increasing attention.

A first step to reduce the RE quantity in the pc-WLED devices is to combine YAG:Ce with a RE-free red phosphor. Manganese ions (Mn^{2+}/Mn^{4+}) are promising candidates thanks to their photoluminescence (PL) properties in the red wavelength range [23, 24]. For example, Mn^{4+}-doped fluoride K_2SiF_6 (KSF) host matrix, allowing a red emission without the use of RE, has been developed by several processes. However, moisture stability and control of the oxidation degree of manganese should be improved though [25].

Quantum dots (QDs) [26] and often more specifically carbon dots (CDs) [27–29] are other promising RE-free materials owing to their narrow PL emission band adjustable over the full visible spectrum thanks to the possible mixing of several different color emitting QDs. Thus, QDs show good potential for white LED phosphors application [30–32]. Nevertheless, they present low quantum yields (QYs) in the solid state and their UV/thermal stability remains unsuitable for commercial requirement for the time being.

Among possible RE-free phosphors, one can also find silica-based luminescent materials such as silicate-carboxylate, silica nanowires and aluminum silicate [33–35]. The decomposition of organic precursors during synthesis or post-synthesis thermal treatments leads to carbon, carbonyl or hydrocarbon defects to which the luminescence is attributed. The same phenomenon has been proposed for yttrium aluminum borate (YAB) synthesized by the modified Pechini process [36]. More recently, for YAB powders prepared by a sol–gel process, we evidenced by involving complementary techniques as ^{13}C labeling nuclear magnetic resonance (NMR)

Journal : 10853 - Large 10853 | Dispatch : 21-8-2022 | Pages : 14
Article No. : 7619 | LE | TYPESET
MS Code : JMSC-D-22-03115R1 | CP | DISK

and electron paramagnetic resonance (EPR) spectroscopies, thermal analyses, optical properties and DFT calculations, that the PL emission originates from polyaromatic hydrocarbon (PAH) molecules entrapped in the inorganic matrix [37–39]. In the same way, larger extended polyaromatic molecules (seven rings and more) with hydroxyl or other oxygenated groups have been proposed as PL emitting centers produced during the successive thermal treatments (pyrolysis and calcination) in the case of modified Pechini-synthesized YAB [40]. Subsequently, the necessity to replace critical elements (yttrium here) from the material composition has led to the study of zinc aluminum borate (ZAB) where not only the glassy network modifier was changed but also the glassy matrix forming elements (aluminum and boron) ratio has been optimized to improve the trapping of the PL emitting centers [41]. Even if borates are known as very interesting optical materials, as highlighted in the recent review [42], their study as rare-earth-free phosphors is rather new and concerns not necessarily crystallized borate matrices.

In this paper, based on our previous results, we eliminate the glass modifier (zinc) from the composition and we describe the development of a rare-earth free phosphor: a luminescent aluminum borate (AB) micrometric powder with a $Al_xB_yO_z$ general formula. The structural and morphological characteristics of this powder have been studied by powder X-ray diffraction (PXRD) and scanning and transmission electron microscopies (SEM—TEM). The stoichiometric precursors ratios used for the syntheses leading to AB powders with the best luminescence properties in terms of PL emission profile and intensity have been determined thanks to optical studies. These latter have been carried out using a near-UV excitation source similar to commercial UV LED chips. Once the precursors ratio optimized, the heating treatment conditions leading to the most suitable AB powder optical properties have been identified. The optical properties have been characterized by recording emission spectra using different excitation wavelengths and performing time-resolved photoluminescence spectroscopy measurements (TRPL).

Experimental

Materials

Citric acid monohydrate was purchased from Sigma-Aldrich (purity 99.0 + %). aluminum nitrate $Al(NO_3)_3{\cdot}9H_2O$ (purity 99.0 + %), D-sorbitol (purity 97.0 + %), boric acid H_3BO_3 (purity 99.8%) and ultrapure water (0.63 µS/cm) were purchased from Fisher Scientific.

Synthesis of AB powder by modified Pechini method

The synthesis of AB luminescent powders has been conducted following the modified Pechini method similar to that already described [41, 43]. Based on these previous works, Fig. 1 illustrates the different preparation steps. Citric acid monohydrate (Cit: 35 to 100.8 mmol) and $Al(NO_3)_3{\cdot}9H_2O$ amounts (Al: 4.2 to 9 mmol) are dissolved in 50 mL of ultrapure water at 80 °C under stirring for 20 min (solution 1). At the same time, D-sorbitol (Sorb: 33.6 to 70 mmol) and H_3BO_3 amounts (B: 12 to 16.8 mmol) are dissolved in the same conditions (solution 2). The powder PL has been optimized by exploring different molar ratios among precursors: the inorganic ratio, R_i = Al/B, the organic ratio, R_o = Cit/Sorb, and the organic/inorganic ratio, $R_{o/i}$ = (Cit + Sorb)/(Al + B). R_i has been studied from 0.25 to 0.75, R_o from 0.5 to 2 and $R_{o/i}$ from 4 to 8. All the ratios are summarized in Table 1.

Solution 1 and solution 2 were mixed together and heated under reflux at 100 °C for 48 h (first step, Fig. 1) leading to a yellowish/orange color solution. This resulting solution was partially evaporated at 80 °C in a ventilated furnace, initiating the polyesterification reactions and subsequently heated at 250 °C for 30 min with a heating rate of 30 °C/h under air. An expanded brown solid was obtained and crushed 5 times by dry planetary milling for 3 min at 430 rpm in a zirconia bowl with 0.5 mm diameter zirconia balls with an air/powder/bead ratio of 1/1/1 by volume (second step, Fig. 1). The fine brown powder was pyrolyzed at 700 °C for 12 h with a HR of 30 °C/h under a continuous N_2 flow (approx. 10 mL/min). These conditions lead to eliminate a large part of organics (69% mass loss measured by thermogravimetric analysis (TGA), Figure S1) without hot spots that could induce inhomogeneities. The black powder resulting from

Journal : 10853 - Large 10853 Dispatch : 21-8-2022 Pages : 14
Article No. : 7619 LE TYPESET
MS Code : JMSC-D-22-03115R1 CP DISK

the pyrolysis was sieved to select grains with a diameter smaller than 25 µm. The final thermal treatment was a calcination under a continuous O_2 flow of 10 mL/min. For a further study, heating rate (HR) and calcination temperature (T_{ca}) were investigated from 20 °C/h to 90 °C/h and from 680 °C to 720 °C, with a dwell time of 10 min, respectively. During this step, a large part of the remaining organic moieties was oxidized leading to 77% mass loss mainly through CO_2 and H_2O (Figure S2). The total mass loss during the thermal treatments (pyrolysis + calcination) reaches 93%. The final powder is beige and luminescent under UV excitation. The thermal treatments conditions presented in Fig. 1 were set according to the study of ZAB powders carried out by Gaffuri et al.[41]. The luminescent AB powder was synthesized at first in these reported conditions and will be subsequently referred as "reference sample."

Characterizations

Microstructural properties

Powder X-ray diffraction PXRD patterns of AB powders were recorded using a Bruker D8 Endeavor diffractometer operating with Cu-Kα radiation (λ = 1.5418 Å) with a goniometer in a symmetrical geometry. The data were collected in a 2θ range with a scan speed of 1°/min.

Thermogravimetric analysis coupled mass spectrometry Differential thermal analysis (DTA), and TGA were carried out with a SETARAM TAG 16 equipment, using 30 mg samples within 100 µL alumina crucibles and a heating rate of 5 °C/min under pure (Airproducts, alphagaz 2) oxygen. These thermal analyses were directly coupled to a HIDEN analytical apparatus (QGA-HAL201-RC) mass spectrometer to analyze the gaseous by-products of decompositions.

Granulometry Grain sizes of powders were measured by laser granulometry with a Malvern

Table 1 Molar ratios of the precursors, aluminum nitrate, boric acid, citric acid and D-sorbitol used for the preparation of the different samples. **a** study of influence R_o ratio with $R_{o/i}$ = 5 **b** study of influence of $R_{o/i}$ ratio with R_o = 1.5

(a)	(R_o)	Al	:	B	:	Cit	:	Sorb
	0.5	1	:	2	:	5	:	10
	0.75	1	:	2	:	6.4	:	8.6
	1	1	:	2	:	7.5	:	7.5
	1.25	1	:	2	:	8.3	:	6.7
	1.5*	***1***	**:**	***2***	**:**	***9***	**:**	***6***
	2	1	:	2	:	10	:	5
(b)	($R_{o/i}$)	Al	:	B	:	Cit	:	Sorb
	4	1	:	2	:	7.2	:	4.8
	5*	***1***	**:**	***2***	**:**	***9***	**:**	***6***
	6	1	:	2	:	10.8	:	7.2
	6.5	1	:	2	:	11.7	:	7.8
	7	1	:	2	:	12.6	:	8.4
	8	1	:	2	:	14.4	:	9.6

**Reference sample:* molar ratio for Cit and Sorb used for YAB and ZAB powders.

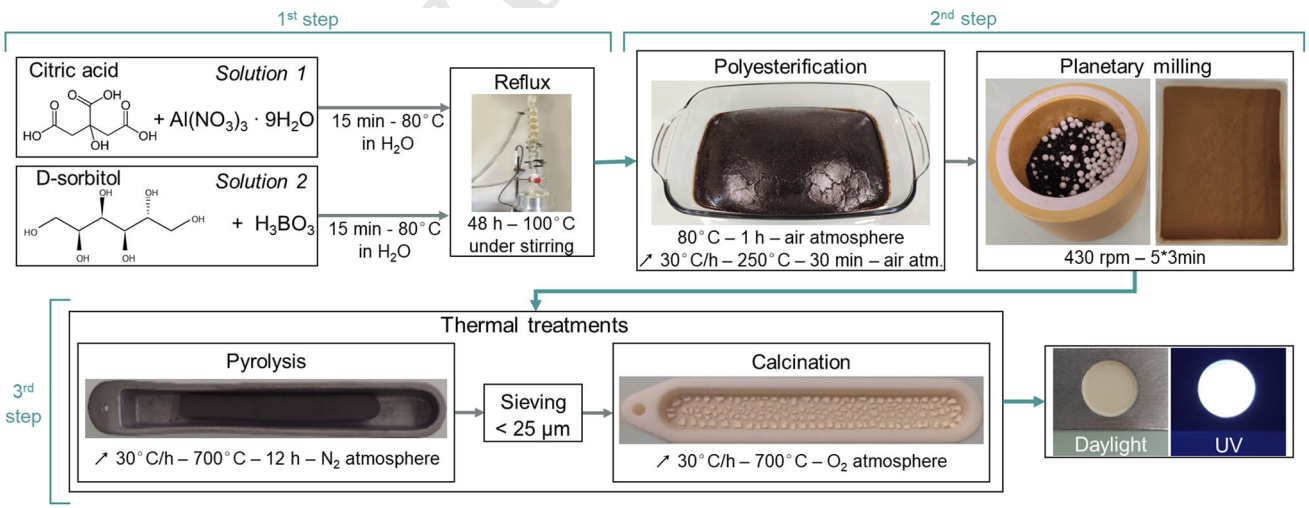

Figure 1 Modified Pechini synthesis of aluminum borate luminescent powders in three major steps.

Journal : 10853 - Large 10853 Dispatch : 21-8-2022 Pages : 14
Article No. : 7619 LE TYPESET
MS Code : JMSC-D-22-03115R1 CP DISK

Mastersizer 2000. Dispersing agent was absolute ethanol.

Microscopy The powder particles have been observed in a field emission scanning electron microscope (FESEM) ZEISS Ultra + . Acceleration voltage V = 2.0 kV & V = 4.0 kV.

Transmission Electronic Microscopy (TEM) images were recorded on a Hitachi H-7650 microscope at the Centre Imagerie Cellulaire Santé (CICS) of Clermont-Ferrand. Acceleration voltage V = 80 kV.

Optical properties Quantum yields & photoluminescence emission QY efficiencies and emission spectra of the powders were measured using a C9920-02G PLQY integrating sphere measurement system from Hamamatsu Photonics. The setup consisted of a 150 W monochromatized Xe lamp, an integrating sphere (Spectralon coating , diameter = 3.3 in) and a high-sensitivity CCD camera. All measurements were carried out at room temperature.

External quantum yield (eQY) was calculated from the internal quantum yield (iQY) and absorption coefficient (Abs) measurements according to Eq. (1):

$$eQY = iQY \times Abs \tag{1}$$

Measurement uncertainties of iQY and Abs are 5% of the measured values, eQY uncertainty arises from:

$$\frac{\Delta eQY}{eQY} = \frac{\Delta iQY}{iQY} + \frac{\Delta Abs}{Abs} \tag{2.1}$$

$$\Delta eQY = \Delta iQY \times Abs + \Delta Abs \times iQY \tag{2.2}$$

$$\Delta eQY = 5\% \times iQY \times Abs + 5\% \times Abs \times iQY \tag{2.3}$$

$$\Delta eQY = 10\% \times eQY \tag{2.4}$$

Time-resolved photoluminescence TRPL was performed at room temperature. The excitation source was the second harmonic (400 nm) of a Ti:Sa pulsed laser with a pulse duration of 150 fs and a repetition rate of 76 MHz. The average power on the sample is equal to 5 W cm^{-2}. The photoluminescence signal was collected in a 32 cm focal monochromator using a grating with 300 gr/mm coupled with a streak camera.

Results and discussion

As noticed in the introduction, Burner et al. identified carbonaceous species, PAHs-type small molecules, as emitting centers of the sol–gel-synthesized YAB powders [37]. The presence of larger PAH molecules as emitting centers was recently confirmed for YAB powders synthesized by the modified Pechini method [40]. Based on this knowledge, we selected several synthesis parameters that seemed relevant to favor the formation of PAH-like molecules trapped in the inorganic matrix to improve the photometric parameters of the AB powders. Therefore, the influence of molar ratios of the different inorganic and organic precursors, as well as the calcination conditions (heating rate and temperature of calcination) were studied. Before presenting the optimization of these parameters using the optical study, the first part of this section will be dedicated to structural and morphological properties of AB powders, that remain identical whatever the precursor ratios.

Grain morphology and structure

SEM images of the typical AB sample were recorded after each synthesis step and are presented with the corresponding PXRD patterns in Fig. 2 to study its structure-morphology relationship. The brown expanded matrix milled in a micron-sized powder has a slight porosity due to the off-gassing occurring during polyesterification reactions (Fig. 2a). On the PXRD pattern (Fig. 2a), a weak peak at 2θ = 28° (indexed by a red up-triangle) is attributed to H_3BO_3 recrystallization. The PXRD pattern of the pyrolyzed powder (Fig. 2b) reveals a totally amorphous material. The SEM images show rough faces and smoother ones, marked by conchoidal fractures (highlighted on the 300-nm-scaled photograph, Fig. 2b), specific to glassy materials. The SEM photograph 3-µm-scaled of AB powder calcined at 700 °C (Fig. 2c) evidences a similar aspect to the pyrolyzed one. The luminescent powder keeps the glassy characteristics evidenced by the conchoidal fractures. Furthermore, some grains present on their surface a thin crust of 10 nm-diameter nanowires (weak surface crystallization, Fig. 2c—confirmed by TEM study, Figure S3) assigned to the $Al_4B_2O_9$ phase according to the corresponding PXRD pattern (Fig. 2c) [41]. On the other hand, the H_3BO_3 partial recrystallization is indicated by the presence of the thin intense peak at 28° (2θ).

Journal : 10853 - Large 10853 Dispatch : 21-8-2022 Pages : 14
Article No. : 7619 LE TYPESET
MS Code : JMSC-D-22-03115R1 CP DISK

This phenomenon may be due to the hydrolysis of the boron in the matrix. The grain size was controlled thanks to the sieving step before calcination and measured by laser granulometry both after pyrolysis (volume-weighted mean diameter, denoted $D_{4,3}$ = 18 µm) and calcination ($D_{4,3}$ = 9 µm) steps (Figure S4). In the following investigations, all powders were assumed to be with similar morphology and granulometry.

Optimization of the inorganic ratio R_i

The network modifiers (Y^{3+} or Zn^{2+} cations) have been removed from the glassy inorganic matrix in this study. Thus, it is important to check the ability of the AB matrix to trap PAH emitting centers. The influence of the Al/B molar ratio was studied starting from the previous results obtained for ZAB powders [41]. Three samples were prepared as described in the experimental section (R_i = 0.25; 0.5; 0.75). Their optical properties have been studied. The eQY of samples calcined at 650 °C, 675 °C, 700 °C and 725 °C was measured for an excitation wavelength of λ_{exc} = 385 nm (Figure S5). The highest eQY (17.9% ± 1.8%) was reached for a R_i = 0.5 calcined at 700 °C. This ratio is associated with a broader and more intense PL emission band than the 0.25 and 0.75 Al/B ratios for the same calcination temperature (Figure S6). Thus, as observed for ZAB matrices, samples with R_i larger than 0.75 were characterized by colder PL emissions and lower eQYs. This confirms that the inorganic precursors ratio affects the formation and trapping mechanisms of the PAH molecules by the aluminum borate matrices. Therefore, the Al/B ratio of 0.5 was selected for the following optimization studies.

Optimization of R_o and $R_{o/i}$ molar ratios

Organic precursors being at the origin of the formation of PAH molecules within the inorganic matrix, the influence of R_o and $R_{o/i}$ ratios on the PL of powders was studied. On one hand, the R_o ratio assesses the importance of both precursors, citric acid (α-hydroxylated tricarboxylic acid) and sorbitol ($C_6H_8(OH)_6$) which play the role of complexing

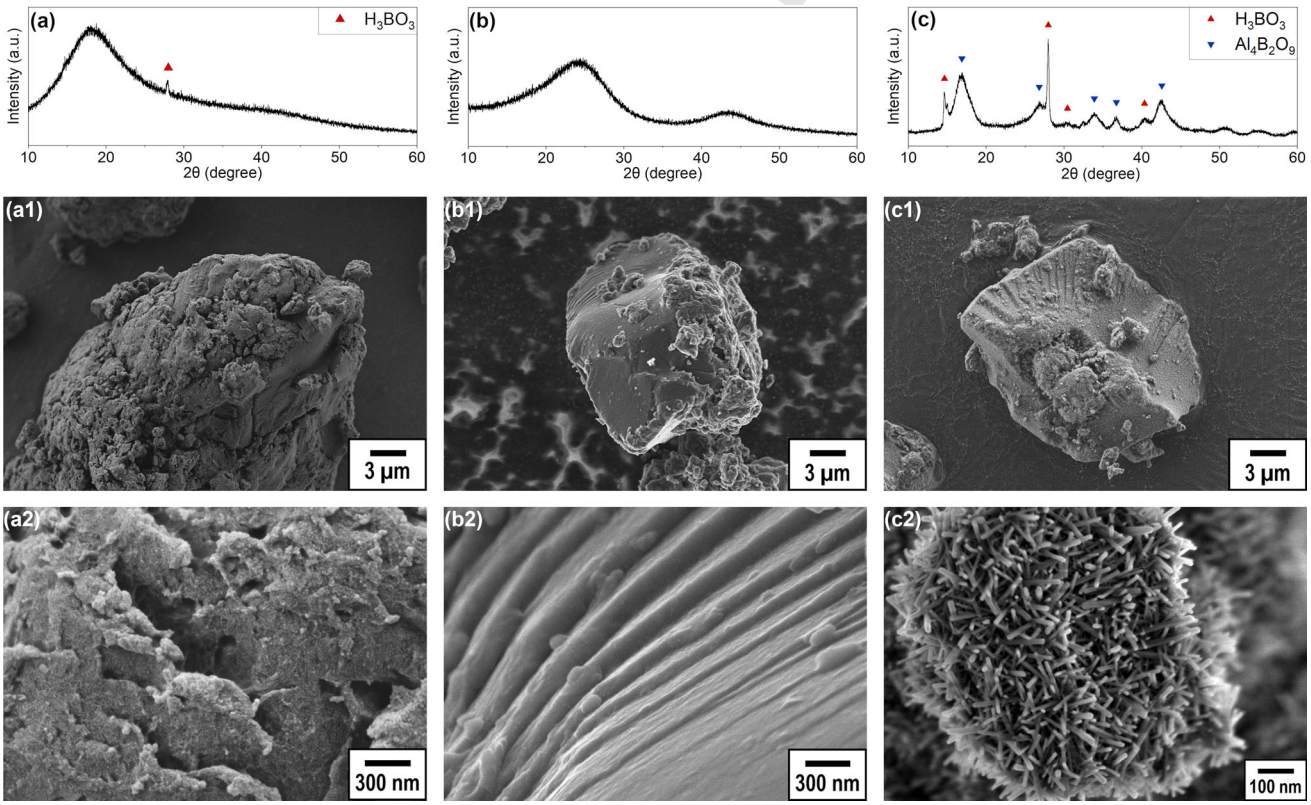

Figure 2 XRD patterns and corresponding SEM images of AB sample after each step of the modified Pechini synthesis: **a a1 a2** brown powder, **b b1 b2** powder pyrolyzed at 700 °C, **c c1 c2** powder calcined at 700 °C.

Journal : 10853 - Large 10853 | Dispatch : 21-8-2022 | Pages : 14
Article No. : 7619 | LE | TYPESET
MS Code : JMSC-D-22-03115R1 | CP | DISK

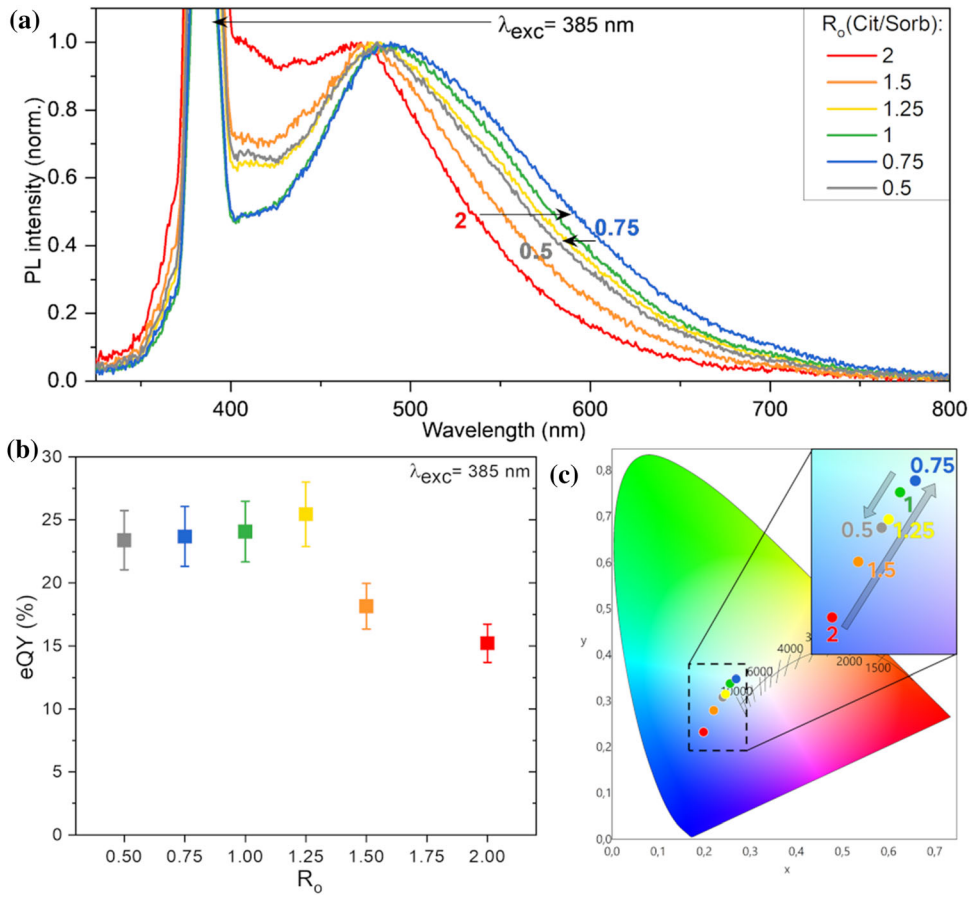

Figure 3 Normalized PL emission spectra (**a**) and corresponding eQYs (**b**) and CIE (Conference Internationale de l'Eclairage 1931) chromaticity coordinates (**c**) of AB samples with R_o ratios varying from 0.5 to 2.

agents of aluminum and boron atoms and allow the formation of the polymer network by esterification between free carboxylic and alcohol functions. On the other hand, the $R_{o/i}$ ratio was adjusted keeping R_o constant in order to evaluate the best quantity of organic compounds to use relative to aluminum and boron forming the inorganic network. The different compositions have been compared with the results obtained for the initial synthetized powder considered as reference. The investigated R_o and $R_{o/i}$ ratios varied from 0.5 to 2 for R_o and from 4 to 8 for $R_{o/i}$, with R_i kept constant at 0.5 (Table 1). The PL properties (emission spectra and QY) of all these samples have been studied to select the ratio leading to the best photometric characteristics.

Figure 3 presents the normalized PL emission spectra of samples with R_o varying from 0.5 to 2 for a fixed $R_{o/i}$ = 5 (reference value, Table 1). The near-UV excitation wavelength has been set to 385 nm since it corresponds to the wavelength of some commercial UV LEDs. The PL emission spectrum of the reference sample (R_o = 1.5, in orange) has a broad emission band lying from the blue to the yellow wavelengths range. Decreasing the R_o from 2 to 0.75 progressively shifts and widens the PL emission spectra to higher emission wavelengths (Fig. 3a). This is confirmed by the CIE chromaticity coordinates: the emission is warmer when R_o decreases from 2 to 0.75 (Fig. 3c). With a lower R_o = 0.5, the PL emission goes backward to a colder color. Corresponding eQYs for the same excitation wavelength (385 nm) are shown in Fig. 3b. The maximum value of the eQY (25.4% ± 2.5%) is obtained for R_o = 1.25. Below this R_o, eQY remains between 23.4% ± 2.3% and 24.1% ± 2.4%. Above this ratio, the eQY decreases to 15.2% ± 1.5%.

In addition, during syntheses, we noticed that R_o below 1 led to the formation of poorly expanded

Journal : 10853 - Large 10853 | Dispatch : 21-8-2022 | Pages : 14
Article No. : 7619 | LE | TYPESET
MS Code : JMSC-D-22-03115R1 | CP | DISK

brown solids with a higher hardness making the grinding and sieving steps more difficult. Thus, the grain size is less controllable. In fact, a low R_o reduces the CO_2 off-gassing resulting from the decarboxylation of the citrate during the heating of the polyesterification step. In conclusion, the $R_o = 1$ seems to be a good compromise to keep an easy-to-grind powder presenting suitable optical properties: an eQY of 24.1% ± 2.4% and still a warmer PL emission than the reference sample.

Alongside, the study concerning the influence of $R_{o/i}$ ratio on powder emission properties is presented in Fig. 4. $R_{o/i}$ ratio increases from 4 to 8 while R_o is kept at the reference value of 1.5. The PL emission spectra (Fig. 4a) are obtained with an excitation wavelength of 385 nm. Increasing the $R_{o/i}$ ratio from 4 to 6.5 makes the PL emission warmer and broader. Beyond 6.5, the PL emission shifts toward the shorter wavelengths. Therefore, the sample for which $R_{o/i}$ ratio is 6.5 generates the warmest and broadest emission band, ranging from 400 to 700 nm. Regarding the eQYs (Fig. 4b), the optimum value is for $R_{o/i} = 7$ (eQY = 22.6% ± 2.3%). However, the best compromise between a rather efficient eQY and a broad and warm PL emission is given by the $R_{o/i}$ ratio of 6.5. Indeed, this $R_{o/i}$ ratio at 6.5 provides a PL emission band significantly shifted by 50 nm toward the long wavelengths in comparison to $R_{o/i} = 7$, while maintaining an eQY of 20.3% ± 2.0%.

Considering these results, an optimized composition was chosen allowing to improve the optical characteristics (colorimetry, quantum efficiency) while maintaining a reproducible synthesis. It is characterized by the following ratios: $R_o = 1$ and $R_{o/i} = 6.5$. Thus, we can guess that the optimization of the carbonated precursors quantities has led to more

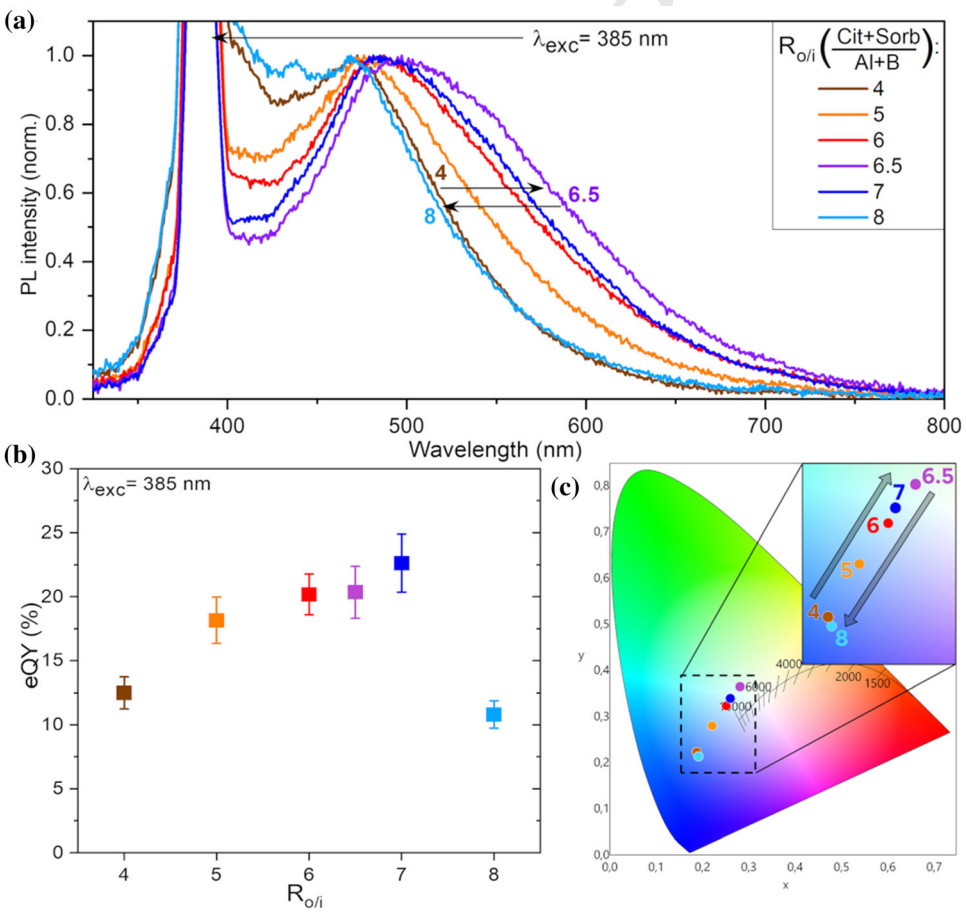

Figure 4 Normalized PL emission spectra (**a**) and corresponding eQYs (**b**) and CIE chromaticity coordinates (**c**) of AB samples with $R_{o/i}$ ratios varying from 4 to 8.

Journal : 10853 - Large 10853 | Dispatch : 21-8-2022 | Pages : 14
Article No. : 7619 | LE | TYPESET
MS Code : JMSC-D-22-03115R1 | CP | DISK

PL emitting centers (PAH molecules) trapped in the aluminum borate matrix while keeping identical the other synthesis conditions.

Optimization of the calcination parameters

Once the precursors composition has been optimized, attention was focused on calcination parameters. This thermal treatment is crucial for the PL emission properties of AB powders. Thermogravimetric analysis coupled mass spectrometry (TGA-MS, Figure S7) shows a 7 wt% loss of water between 100 and 200 °C demonstrating the slight hygroscopicity of the powder. The main mass loss of 73 wt% for the temperature range 450–600 °C is related to the decomposition of the pyrolytic carbon eliminated by oxidation (CO_2, CO and H_2O exhaust gases). In addition, this thermal treatment leads to the trapping of emitting centers formed within the inorganic matrix when it densifies. Thus, the oxidation conditions of pyrolyzed powders induce variations in the PL emission profiles and in photometric characteristics of the AB powders. Therefore, we optimized the calcination conditions by varying the HR and the final T_{ca} around previously defined values (HR = 30 °C/h and T_{ca} = 700 °C).

The HR variation keeping the same final reference temperature of 700 °C was first studied. Figure 5 shows the results of PL emissions and eQY versus HR. The three circular photographs in Fig. 5 correspond to the calcined powders prepared with HR = 20, 40 and 90 °C/h. For a slow HR (20 °C/h), the obtained yellowish-colored powder exhibits a narrow PL emission in the blue range and a moderate eQY. In this case, the long heating time to reach the final T_{ca} (700 °C) is associated to a slow formation and densification of the aluminum borate matrix. This favors the strong oxidation of the previously pyrolyzed powder. Thus, a part of the emitting centers (PAHs) has been degraded by the long oxidation step, in particular those emitting in the yellow range. On the opposite, the powder calcined through high HR (90 °C/h) has been partially oxidized exhibiting a grayish color due to the significant presence of black carbon. The fast heating treatment must have favored the rapid densification of the AB inorganic matrix. This did not allow to sufficiently oxidize a part of the pyrolytic carbon, which thus remained trapped in the aluminum borate network. The residual black carbon species act as non-radiative absorbing centers resulting in low PL efficiency (eQY = 5% ± 0.5%). Intermediate HR value (40 °C/h) leads to beige powder exhibiting the maximum of eQY (20.8% ± 2.1%) and the widest PL emission in the visible range (Fig. 5). We can therefore consider that this HR corresponds to an optimized residence time in the furnace, leading to the best calcination conditions with the simultaneous formation of the AB matrix and a wide range of emitting centers.

We adjusted the final temperature of calcination T_{ca} using the optimized heating rate HR = 40 °C/h. A third 2.8 wt% mass loss close to 700 °C (Figure S7) is related to carbon elimination, particularly originated from the emitting centers trapped until then in the matrix. As a consequence, we have studied AB powders obtained with a T_{ca} comprised between 680 °C and 720 °C, taking into account that for higher T_{ca} the emission intensity significantly decreases

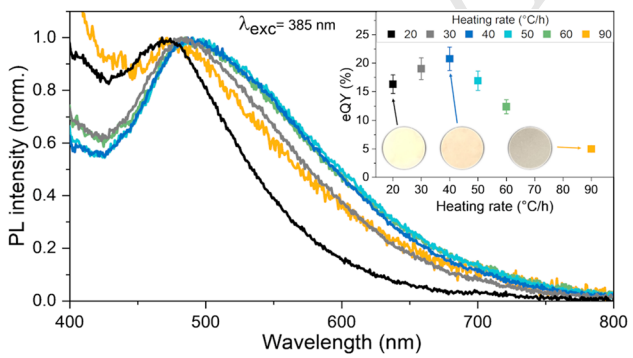

Figure 5 Normalized PL emission spectra and corresponding eQYs of AB samples calcined at different HR (from 20 °C/h to 90 °C/h) to the T_{ca} of 700 °C. Three round photographs of the powders calcined, respectively, at 20 °C/h, 40 °C/h and 90 °C/h are presented in the eQY graph.

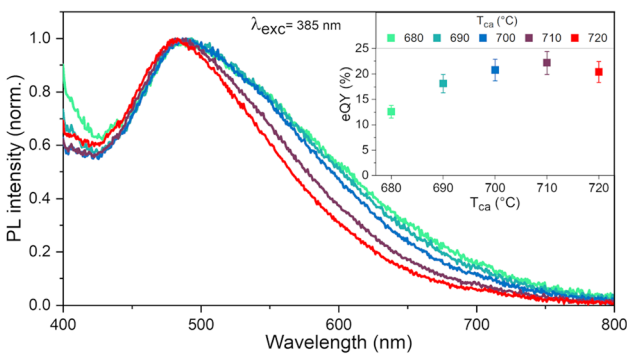

Figure 6 Normalized PL emission spectra and corresponding eQYs of AB samples calcined at different T_{ca} values from 680 °C to 720 °C with HR = 40 °C/h.

Journal : 10853 - Large 10853 Dispatch : 21-8-2022 Pages : 14
Article No. : 7619 LE TYPESET
MS Code : JMSC-D-22-03115R1 CP DISK

while the emission band shifts toward blue wavelengths. Their optical features are gathered in Fig. 6.

It evidences that the best compromise to get a warm broad emission together with a satisfying eQY is to calcine the AB sample at 700 °C. Indeed, even if the eQY maximum is reached with T_{ca} = 710 °C, the emission bandwidth is significantly reduced above 700 °C. Below 700 °C, the emission bandwidth is almost not affected, but the eQY is quite lower indicating a less-efficient transformation of PAH molecules. Thus, the evolution in photometric characteristics are mainly related to the one of the PAH nature through partial oxidation during the calcination [40] (as hydroxylated PAH) before elimination at higher temperature (720 °C).

In conclusion, the optimized calcination conditions are a HR of 40 °C/h and a temperature T_{ca} of 700 °C. The next part of this work will be dedicated to the use of TRPL to study the origin of the PL and the differences that may arise from the changes in the precursors ratio.

Time-resolved photoluminescence

TRPL analyses have been conducted on the optimized AB powder (Fig. 7) and the reference sample (see Table 1 for composition and Figure S9 for the decays) at the excitation wavelength of 400 nm. Three emission wavelengths have been studied: 448 nm for the blue contribution, 506 nm corresponding to the maximum of emission and 563 nm for the yellow contribution of the emission spectrum. The data were normalized and fitted with a bi-exponential decay Eq. (3):

$$y = A_1 \exp\left(\frac{-t}{\tau_1}\right) + A_2 \exp\left(\frac{-t}{\tau_2}\right) \quad (3)$$

τ1 and τ2 are the short and long lifetimes, respectively. A1 and A2 are the weights corresponding to each part of the decay. Figure 7 shows the results obtained thanks to the bi-exponential fitting for the three emission wavelengths studied. The results of the fit are gathered in Table 2.

The TRPL measurements of AB powders suggest the presence of several types or sizes [44] of emitting species as they are characterized by two decay lifetimes. The optimized sample decay curve for the 448 nm emission wavelength is characterized by quite equiponderant contributions of 45% and 55%, respectively, for the short lifetime (τ1 = 0.7 ± 0.1 ns) and the long lifetime (τ2 = 2.4 ± 0.1 ns). For emission wavelength in the green range (λ_{em} = 506 nm), the long lifetime is more weighted with 60%, and both short and long time constants present increased values compared with the blue wavelength decay: τ1 = 0.9 ± 0.1 ns and τ2 = 2.8 ± 0.1 ns. The trend continues for the yellow emission wavelength (λ_{em} = 563 nm), with A1 = 30% and A2 = 70%, the short lifetime weight is reduced for the benefit of the long lifetime. This tendency is well noticeable in Fig. 7, as well as the evolution of τ1 and τ2 whose both values increase to 1.4 ± 0.1 ns and 3.6 ± 0.1 ns, respectively. The evolution of the values and the weights of τ1 and τ2 with the different emission wavelengths supports the hypothesis of the presence of several types or sizes of PAH emitting centers.

The behavior of the decays of the reference sample (Figure S9, Table 2) is very analogous to the one of the optimized samples. If this similarity of the lifetimes suggests that the nature of the emitting centers of the reference and optimized powders are close, the improvements of eQY and the broadening with bathochromic effect should be attributed to the quantity of emitting centers and to their fashion of trapping in the inorganic matrix.

The final part of this work will highlight the tunability of the emission features of the AB powders depending on the excitation wavelength.

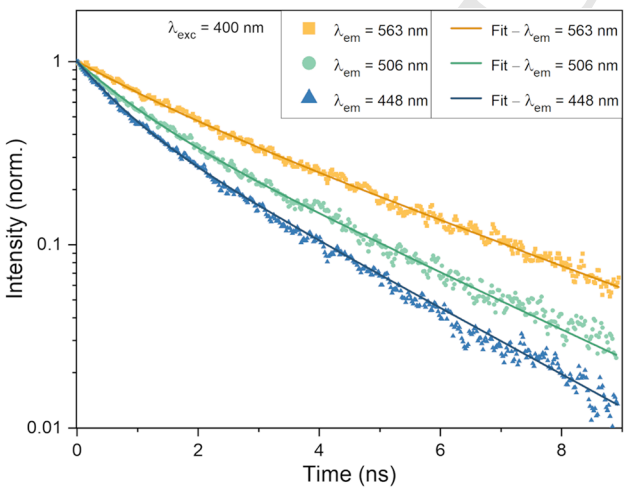

Figure 7 Room-temperature decay curves of optimized AB powder recorded under 400 nm-excitation for different emission wavelengths.

Journal : 10853 - Large 10853 Dispatch : 21-8-2022 Pages : 14
Article No. : 7619 LE TYPESET
MS Code : JMSC-D-22-03115R1 CP DISK

Table 2 Short and long lifetimes (τ1, τ2) and associated weights (A1, A2) obtained by fitting (bi-exponential decay) the TRPL data of optimized and reference AB powders excited at 400 nm, for three emission wavelengths (448 nm, 506 nm and 563 nm)

Sample	λ_{em} (nm)	τ1 (ns)	τ2 (ns)	A1 (%)	A2 (%)	R^2
Optimized	448	0.7 ± 0.1	2.4 ± 0.1	45	55	0.9985
	506	0.9 ± 0.1	2.8 ± 0.1	40	60	0.9975
	563	1.4 ± 0.1	3.6 ± 0.1	30	70	0.9974
Reference	448	0.6 ± 0.1	2.4 ± 0.1	46	54	0.9980
	506	0.9 ± 0.1	2.9 ± 0.1	40	60	0.9984
	563	1.2 ± 0.1	3.6 ± 0.1	32	68	0.9965

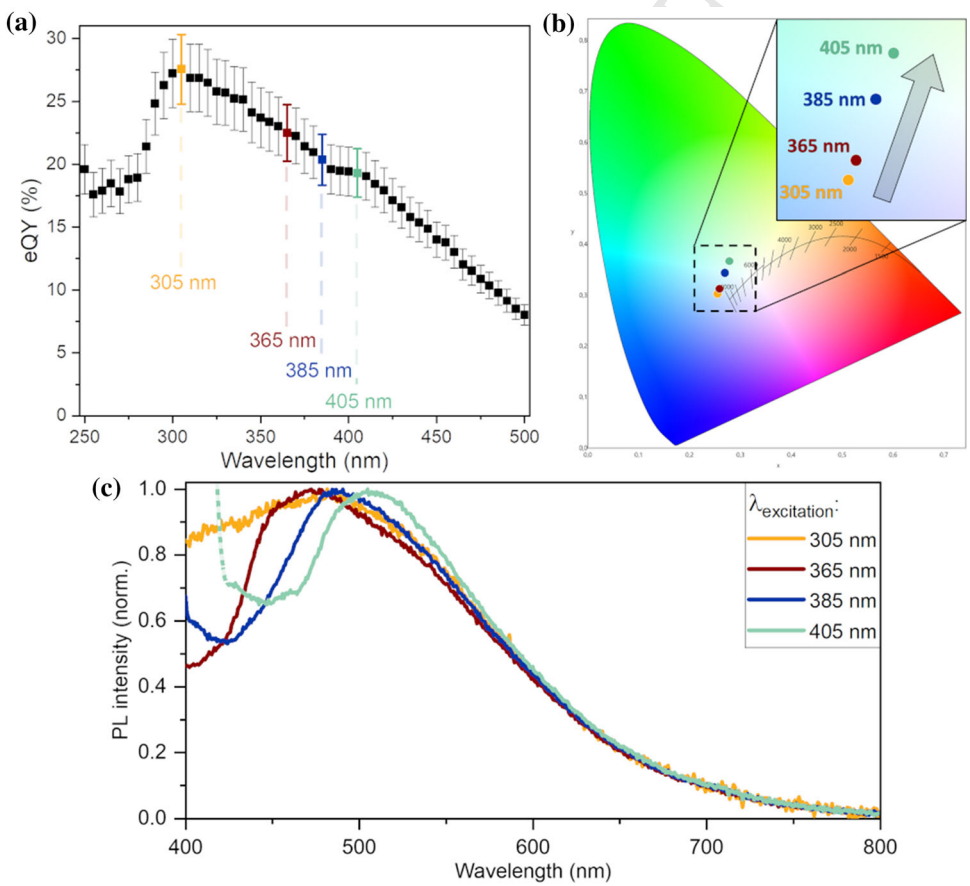

Figure 8 eQYs (**a**), corresponding CIE coordinates (**b**) and normalized PL emission spectra (**c**) of optimized AB powder with focus on the maximum eQY value at 305 nm and usual near-UV chip wavelengths at 365, 385 and 405 nm..

Excitation wavelength modulation

The AB luminescent powders offer a particularly interesting characteristic: they can be excited in a wide range of wavelengths from UV to blue wavelengths as illustrated for the optimized powder in Fig. 8a. Thus, the most-used commercial UV wavelengths (365 nm, 385 nm, 405 nm) are included in this excitation domain. The maximum eQY is 27.6% ± 2.8% for λ_{exc} = 305 nm. The corresponding PL emission spectrum and those measured with λ_{exc} = 365 nm, 385 nm and 405 nm are presented in Fig. 8c. The associated CIE chromaticity coordinates (Fig. 8b) highlight the bathochromic emission shift occurring for the same sample when the excitation wavelength increases.

This tunable emission profile could be explained by the existence of PAHs of different sizes, such as coronene or circumcoronene molecules as recently evidenced by Salaün et al. combining spectroscopic results (PL, EPR) and DFT calculations [40]. This specific behavior is particularly interesting for tuning

Journal : 10853 - Large 10853 Dispatch : 21-8-2022 Pages : 14
Article No. : 7619 LE TYPESET
MS Code : JMSC-D-22-03115R1 CP DISK

the white emission from pretty cold to pretty warm color, including AB powders in a device combining different kinds of UV-LEDs.

Conclusion

In this work, RE-free AB phosphors presenting a broad PL emission band in the visible range under near-UV excitation have been developed by a modified Pechini process. Their PL properties are due to the presence of PAH emitting centers trapped in the inorganic matrix. The different steps of the synthesis have been optimized to improve the photometric properties of AB powders. Both inorganic and organic precursors molar ratios were optimized. Respectively, Al/B = 0.5, Cit/Sorb = 1 and (Cit + Sorb)/(Al + B) = 6.5 are the ratios for which PL emission is the widest and warmest (from 400 to 700 nm) with near-UV excitation (385 nm). The trapping properties of the inorganic AB matrix were enhanced, while the formation of PAH molecules emitting at warmer wavelengths was promoted. Then, the parameters of the calcination treatment, under O_2 atmosphere, were adjusted. During this last synthesis step, the oxidation of organic residues resulting from the previous pyrolysis and acting as absorbing centers, is completed. The best conditions allowing a suitable oxidation step leading to the formation and conservation of emitting centers were determined: a heating rate of 40 °C/h and a calcination temperature of 700 °C. TRPL measurements were performed to characterize the PAH emitting centers in the solid state. The optimized powder presents a satisfying eQY from 19 to 28% on a wide range of UV-excitation wavelengths (from 305 to 405 nm). Moreover, the possibility of adapting the excitation wavelength to get an emission band with controlled profile has been described. It is quite interesting for applications in which the color of emission needs to be tuned in a condensed device with a single phosphor associated to several UV-excitation sources.

Acknowledgment

The authors thank Christelle Blavignac (Centre Imagerie Cellulaire Santé – Université Clermont Auvergne, France) for her technical support for TEM observations.

Funding

This work was carried out under Région Auvergne Rhône Alpes, Pack Ambition Recherche 2019, "LUMINOLED" project.

Declarations

Conflict of interest The authors declare that they have no conflict of interest.

Supplementary Information: The online version contains supplementary material available at https://doi.org/10.1007/s10853-022-07619-5.

References

[1] Nair GB, Swart HC, Dhoble SJ (2020) A review on the advancements in phosphor-converted light emitting diodes (pc-LEDs): Phosphor synthesis, device fabrication and characterization. Prog Mater Sci 109:100622. https://doi.org/10.1016/j.pmatsci.2019.100622

[2] Yang L, Chen M, Lv Z et al (2013) Preparation of a YAG: Ce phosphor glass by screen-printing technology and its application in LED packaging. Opt Lett 38:2240. https://doi.org/10.1364/OL.38.002240

[3] Cho J, Park JH, Kim JK, Schubert EF (2017) White light-emitting diodes: History, progress, and future: White light-emitting diodes. Laser Photon Rev 11:1600147. https://doi.org/10.1002/lpor.201600147

[4] Ye S, Xiao F, Pan YX et al (2010) Phosphors in phosphor-converted white light-emitting diodes: recent advances in materials, techniques and properties. Mater Sci Eng R Rep 71:1–34. https://doi.org/10.1016/j.mser.2010.07.001

[5] Hu Y, Zhuang W, Ye H et al (2005) Preparation and luminescent properties of (Ca1-x, Srx)S:Eu2+ red-emitting phosphor for white LED. J Lumin 111:139–145. https://doi.org/10.1016/j.jlumin.2004.07.005

[6] Pricha I, Rossner W, Moos R (2016) Layered ceramic phosphors based on $CaAlSiN_3$: Eu and YAG: Ce for white light-emitting diodes. J Am Ceram Soc 99:211–217. https://doi.org/10.1111/jace.13948

[7] Jargus V, Nedoma, et al (2019) Effect of selected luminescent layers on CCT, CRI, and response times. Materials 12:2095. https://doi.org/10.3390/ma12132095

Journal : 10853 - Large 10853 | Dispatch : 21-8-2022 | Pages : 14
Article No. : 7619 | LE | TYPESET
MS Code : JMSC-D-22-03115R1 | CP | DISK

[8] Fukui T, Kamon K, Takeshita J et al (2009) Superior illuminant characteristics of color rendering and luminous efficacy in multilayered phosphor conversion white light sources excited by near-ultraviolet light-emitting diodes. Jpn J Appl Phys 48:112101. https://doi.org/10.1143/JJAP.48.112101

[9] Li R, Li H, Peng Y, et al (2016) Development of RGB phosphor-in-glass for ultraviolet-excited white light-emitting diodes packaging. In: 2016 17th International Conference on Electronic Packaging Technology (ICEPT). IEEE, Wuhan, China, pp 94–97

[10] Peng Y, Cheng H, Chen Z, Li R (2016) Multi-layered Red, Green, and Blue Phosphor-in- Glass for Ultraviolet-Excited White Light-Emitting Diodes Packaging. Th Int Conf Electron Packag Technol 4

[11] Shang M, Li C, Lin J (2014) How to produce white light in a single-phase host? Chem Soc Rev 43:1372–1386. https://doi.org/10.1039/C3CS60314H

[12] Smet PF, Parmentier AB, Poelman D (2011) Selecting conversion phosphors for white light-emitting diodes. J Electrochem Soc 158:R37. https://doi.org/10.1149/1.3568524

[13] Bachmann V, Ronda C, Meijerink A (2009) Temperature quenching of yellow Ce $^{3+}$ luminescence in YAG:Ce. Chem Mater 21:2077–2084. https://doi.org/10.1021/cm8030768

[14] Ivanovskikh KV, Ogiegło JM, Zych A et al (2013) Luminescence temperature quenching for Ce $^{3+}$ and Pr $^{3+}$ *d-f* emission in YAG and LuAG. ECS J Solid State Sci Technol 2:R3148–R3152. https://doi.org/10.1149/2.011302jss

[15] European Comission (2016) Critical raw materials. In: Intern. Mark. Ind. Entrep. SMEs - Eur. Comm. https://ec.europa.eu/growth/sectors/raw-materials/specific-interest/critical_en. Accessed 13 Apr 2022

[16] Golev A, Scott M, Erskine PD et al (2014) Rare earths supply chains: Current status, constraints and opportunities. Resour Policy 41:52–59. https://doi.org/10.1016/j.resourpol.2014.03.004

[17] Ali S (2014) Social and environmental impact of the rare earth industries. Resources 3:123–134. https://doi.org/10.3390/resources3010123

[18] Binnemans K, Jones PT, Blanpain B et al (2013) Recycling of rare earths: a critical review. J Clean Prod 51:1–22. https://doi.org/10.1016/j.jclepro.2012.12.037

[19] Rare Earths Statistics and Information. https://www.usgs.gov/centers/nmic/rare-earths-statistics-and-information. Accessed 13 Apr 2022

[20] (2020) How Rare-Earth Mining Has Devastated China's Environment. In: EarthOrg - Past Present Future. https://earth.org/rare-earth-mining-has-devastated-chinas-environment/. Accessed 13 Apr 2022

[21] Liang T, Li K, Wang L (2014) State of rare earth elements in different environmental components in mining areas of China. Environ Monit Assess 186:1499–1513. https://doi.org/10.1007/s10661-013-3469-8

[22] Pan Y, Li H (2016) Investigating heavy metal pollution in mining brownfield and its policy implications: a case study of the Bayan Obo rare Earth Mine, Inner Mongolia, China. Environ Manage 57:879–893. https://doi.org/10.1007/s00267-016-0658-6

[23] Duan CJ, Delsing ACA, Hintzen HT (2009) Photoluminescence properties of novel red-emitting Mn $^{2+}$ -Activated MZnOS (M = Ca, Ba) phosphors. Chem Mater 21:1010–1016. https://doi.org/10.1021/cm801990r

[24] Chen D (2016) A review on Mn4+ activators in solids for warm white light-emitting diodes. RSC Adv 12

[25] Kumar V, Potdevin A, Boutinaud P, Boyer D (2020) HF-free synthesis of K2SiF6 and BaSiF6 nanoparticles by thermal decomposition. Mater Lett 261:127123. https://doi.org/10.1016/j.matlet.2019.127123

[26] Kurtin J (2013) Quantum dot LED phosphors: performance and reliability improvements. In: Streubel KP, Jeon H, Tu L-W, Strassburg M (eds) San Francisco. California, USA, p 86411D

[27] Wang J, Yang Y, Liu X (2020) Solid-state fluorescent carbon dots: quenching resistance strategies, high quantum efficiency control, multicolor tuning, and applications. Mater Adv 1:3122–3142. https://doi.org/10.1039/D0MA00632G

[28] Guo X, Wang C-F, Yu Z-Y et al (2012) Facile access to versatile fluorescent carbon dots toward light-emitting diodes. Chem Commun 48:2692. https://doi.org/10.1039/c2cc17769b

[29] Zhu J, Shao H, Bai X et al (2018) Modulation of the photoluminescence in carbon dots through surface modification: from mechanism to white light-emitting diodes. Nanotechnology 29:245702. https://doi.org/10.1088/1361-6528/aab9d6

[30] Xie Z, Yin Z, Wu Y et al (2017) White light-emitting diodes based on individual polymerized carbon nanodots. Sci Rep 7:12146. https://doi.org/10.1038/s41598-017-12083-2

[31] Zhu J, Bai X, Zhai Y et al (2017) Carbon dots with efficient solid-state photoluminescence towards white light-emitting diodes. J Mater Chem C 5:11416–11420. https://doi.org/10.1039/C7TC04155A

[32] Onal A, Eren GO, Sadeghi S et al (2022) High-performance white light-emitting diodes over 150 lm/W using near-unity-emitting quantum dots in a liquid matrix. ACS Photon Acsphoton. https://doi.org/10.1021/acsphotonics.1c01805

[33] Green WH (1997) White phosphors from a silicate-carboxylate sol-gel precursor that lack metal activator ions.

Journal : 10853 - Large 10853 | Dispatch : 21-8-2022 | Pages : 14
Article No. : 7619 | LE | TYPESET
MS Code : JMSC-D-22-03115R1 | CP | DISK

Science 276:1826–1828. https://doi.org/10.1126/science.276.5320.1826

[34] Davies G-L, McCarthy JE, Rakovich A, Gun'ko YK (2012) Towards white luminophores: developing luminescent silica on the nanoscale. J Mater Chem 22:7358. https://doi.org/10.1039/c2jm16086b

[35] Hayakawa T, Hiramitsu A, Nogami M (2003) White light emission from radical carbonyl-terminations in Al2O3–SiO2 porous glasses with high luminescence quantum efficiencies. Appl Phys Lett 82:2975–2977. https://doi.org/10.1063/1.1569038

[36] Guimarães VF, Maia LJQ, Gautier-Luneau I et al (2015) Toward a new generation of white phosphors for solid state lighting using glassy yttrium aluminoborates. J Mater Chem C 3:5795–5802

[37] Burner P, Sontakke AD, Salaün M et al (2017) Evidence of organic luminescent centers in Sol–Gel-synthesized yttrium aluminum borate matrix leading to bright visible emission. Angew Chem Int Ed 56:13995–13998. https://doi.org/10.1002/anie.201706070

[38] Sontakke AD, Ferrier A, Burner P et al (2017) Afterglow luminescence in wet-chemically synthesized inorganic materials: ultra-long room temperature phosphorescence instead of persistent luminescence. J Phys Chem Lett 8:4735–4739. https://doi.org/10.1021/acs.jpclett.7b01702

[39] Sontakke AD, Mouesca J-M, Castaing V et al (2018) Time-gated triplet-state optical spectroscopy to decipher organic luminophores embedded in rigid matrices. Phys Chem Chem Phys 20:23294–23300. https://doi.org/10.1039/C8CP03952F

[40] Salaün M, Sontakke AD, Maurel V et al (2022) Relation between material structure and photoluminescence properties in yttrium–aluminum borates phosphors. MRS Bull 47:231–242. https://doi.org/10.1557/s43577-021-00195-0

[41] Gaffuri P, Salaün M, Gautier-Luneau I et al (2020) Rare-earth-free zinc aluminium borate white phosphors for LED lighting. J Mater Chem C 8:11839–11849. https://doi.org/10.1039/D0TC02196B

[42] Mutailipu M, Poeppelmeier KR, Pan S (2021) Borates: a rich source for optical materials. Chem Rev 121:1130–1202. https://doi.org/10.1021/acs.chemrev.0c00796

[43] Guimarães VF, Salaün M, Burner P et al (2017) Controlled preparation of aluminum borate powders for the development of defect-related phosphors for warm white LED lighting. Solid State Sci 65:6–14. https://doi.org/10.1016/j.solidstatesciences.2016.12.011

[44] Ehrat F, Bhattacharyya S, Schneider J et al (2017) Tracking the source of carbon dot photoluminescence: aromatic domains versus molecular fluorophores. Nano Lett 17:7710–7716. https://doi.org/10.1021/acs.nanolett.7b03863

Journal : 10853 - Large 10853 | Dispatch : 21-8-2022 | Pages : 14
Article No. : 7619 | ☐ LE | ☐ TYPESET
MS Code : JMSC-D-22-03115R1 | ☑ CP | ☑ DISK